

ORIGINAL ARTICLE

Open Access



# Lateral resistance and restoring force model of timber frames with traditional joints in Tang, Song, and Qing dynasties

Xinran Li<sup>1</sup>, Shuo Wang<sup>1</sup>, Zhiyuan Chen<sup>1</sup>, Zeli Que<sup>1\*</sup>  and Kohei Komatsu<sup>2</sup>

## Abstract

The mortise–tenon joints in ancient Chinese timber buildings have a significant impact on their lateral resistance. To explore the lateral resistance of timber frames with different mortise–tenon joint connections, this study references existing ancient timber buildings from the Tang, Song, and Qing Dynasties in China. Three different double-span timber frames with different mortise–tenon joint connections were designed and subjected to quasi-static tests under a vertical load of 45 kN. The study analyzes the effects of mortise–tenon joints on the hysteresis curve, envelope curve, stiffness degradation, and energy dissipation capacity of the timber frames. The results show that all timber frames exhibit good deformation recovery capability, and the mortise–tenon joints can withstand significant lateral displacement of the frames. The Qing frame has stronger resistance to deformation and higher energy dissipation, with its maximum restoring force 1.76 times that of the Tang frame and 2.04 times that of the Song frame, but it also experiences faster stiffness degradation. The Tang and Song frames exhibit similar energy dissipation capabilities, but the Tang frame shows higher stiffness and maximum restoring force, while the Song frame has stronger deformation resistance and fuller hysteresis loops. Based on the experimental results, a restoring force model was established for timber frames with different mortise–tenon joint connections.

**Keywords** Mortise–tenon joints, Restoring force model, Ancient Chinese timber buildings, Lateral resistance

## Introduction

Chinese ancient buildings, as precious heritage of Chinese civilization, carry rich cultural connotations. Among them, timber buildings hold a significant place in the existing ancient buildings. Given China's susceptibility to earthquakes, studying the seismic performance of ancient timber buildings is crucial for their preservation. The timber frame is a key component of these buildings' seismic performance, and its lateral resistance is of great importance for the overall seismic study of the structure.

It is well known that ancient Chinese timber buildings have excellent lateral resistance due to the mortise–tenon joints used in construction. Different types of mortise–tenon joints affect the lateral resistance of timber frames to varying degrees, and these joints exhibit distinct characteristics across different historical periods.

In Tang dynasty timber buildings, *Zhi* mortise–tenon joints were commonly employed. These joints intersect with the column heads without reducing thickness [1]. The early Song Dynasty continued the use of Tang methods for mortise–tenon joints, but regional differences led to variations in wall structures and, consequently, in the binding capabilities of the joints. Therefore, in early Song Dynasty, northern timber buildings commonly used *Zhi* mortise–tenon joints, while southern timber buildings often used mortise–tenon joints with stronger binding capability, such as

\*Correspondence:

Zeli Que  
zelique@njfu.edu.cn

<sup>1</sup> College of Material Science and Engineering, Nanjing Forestry University, Nanjing 210037, Jiangsu, China

<sup>2</sup> Research Institute for Sustainable Humosphere, Kyoto University, Kyoto 611-0011, Japan



© The Author(s) 2025. **Open Access** This article is licensed under a Creative Commons Attribution 4.0 International License, which permits use, sharing, adaptation, distribution and reproduction in any medium or format, as long as you give appropriate credit to the original author(s) and the source, provide a link to the Creative Commons licence, and indicate if changes were made. The images or other third party material in this article are included in the article's Creative Commons licence, unless indicated otherwise in a credit line to the material. If material is not included in the article's Creative Commons licence and your intended use is not permitted by statutory regulation or exceeds the permitted use, you will need to obtain permission directly from the copyright holder. To view a copy of this licence, visit <http://creativecommons.org/licenses/by/4.0/>.

*Yanwei* mortise–tenon joint [2]. It should be noted that the main hall of Baoguo Temple in Ningbo, China uses the *Niekou gumao* mortise–tenon joint recorded in the *Yingzao Fashi* (A.D.1103, Song Dynasty) [3]. Currently, only two building examples of this joint remain, making it particularly valuable for research [4]. In Ming and Qing Dynasty buildings, the *Yanwei* mortise–tenon joint is the primary form of mortise–tenon joint [5]. Besides the *Yanwei* mortise–tenon joint, the *Gutou* mortise–tenon joint is also commonly used in Ming and Qing Dynasty buildings, primarily at the intersections of *Fangs* (a horizontal component in ancient Chinese building) and columns at their ends and corners [6]. The embracing shoulder style mortise–tenon joint also gradually became popular in the mid to late Ming period. This method enhanced the structural functionality of the joint and reduced the shear force on the tenon root [7]. Analysis reveals that the mortise–tenon joints from the Tang (A.D.618–907), Song (A.D.960–1276), and Qing (A.D.1644–1911) Dynasties exhibit distinct characteristics of their respective eras. Given the significant time span covered by these periods in the history of Chinese architecture, they provide a useful basis for comparing the mechanical properties of mortise–tenon joints and their impact on lateral resistance of timber frames across different historical periods.

In recent years, researchers have conducted extensive experimental studies on *Yanwei* mortise–tenon joints and *Zhi* mortise–tenon joints. They have used single joint models [5, 8, 9] to carry out monotonic loading tests or quasi-static tests, analyzing the failure modes and mechanical properties of the joints. Xue et al. conducted quasi-static tests on single joint models of *Yanwei* mortise–tenon joints and *Tou* mortise–tenon joints. The results showed that the *Tou* mortise–tenon joint was lower than that of *Yanwei* mortise–tenon joint. Moreover, the two types of mortise–tenon joints exhibit different stiffness degradation patterns [10]. Chun et al. compared the mechanical properties of various mortise–tenon joints and approximated the skeleton curves of these joints as a three-linear model [2]. Based on experimental studies, researchers have also fitted restoring force models for *Yanwei* mortise–tenon, through mortise–tenon, and half tenon joints [5, 11]. The ancient timber buildings in East Asia have certain similarities. According to a study conducted by Li et al., the resistance of deep beams is affected by beam–column joints, and the axial force of the deep beam, in turn, retards beam–column joint damage [12]. Studies on Japan's "*Nuki*" joints indicate that the force conditions of the joints affects their moment, stiffness

degradation, and energy dissipation capabilities [13]. Therefore, conducting tests on timber frames can better simulate the actual force conditions of the joints, providing a more accurate mechanical performance of mortise–tenon joints.

The column frame is the main load-bearing structure in ancient Chinese timber buildings, consisting of columns and *Fangs* connected by mortise–tenon joints [14]. Research has shown that the energy dissipation of the column frame is the primary mode of energy dissipation in ancient timber buildings. As the earthquake intensity increases, the proportion of energy dissipated by the column frame within the overall structure also rises. Thus, the energy dissipation capability of the column frame plays a decisive role in the energy dissipation of ancient timber building [15]. In recent years, many scholars have conducted numerous quasi-static tests on timber frames connected by *Yanwei* mortise–tenon joints and *Zhi* mortise–tenon joints. The timber frame forms include single-span [16], double-span [17], and four-*Fang*–four-column [15], with the single-span model being the most studied. The deformation mode of timber frames exhibits a rocking deformation, with hysteresis curves showing an S-shape [15, 18]. As the horizontal displacement increases, the slip amount of the mortise–tenon joints also increases. Researchers have established restoring force models based on characteristic parameters obtained from test results, such as yield points, peak load points, and stiffness, to characterize the hysteresis performance of timber frames [15, 19]. These restoring force models showed good consistency with the test results. However, current research on timber frames often uses single-span models and typically uses *Yanwei* or *Zhi* mortise–tenon joints. There are limited types of models, and comparative studies on timber frames connected by different mortise–tenon joints are scarce. In addition, restoring force models for joints and timber frames are mostly based on *Yanwei* or *Zhi* joints, limiting their applicability.

This paper examined typical examples of existing timber buildings from the Tang, Song, and Qing Dynasties and designed three double-span timber frames connected by different mortise–tenon joints. Through quasi-static tests, the hysteresis curves, envelop curves, stiffness degradation, and energy dissipation of the timber frames were analyzed. The objective is to compare the lateral resistance of three timber frames and to propose a restoring force model applicable to timber frames with different mortise–tenon joint connections. The findings aim to provide a reference for establishing theoretical analysis models of timber frames and to assist in the assessment and reinforcement of existing ancient timber buildings.

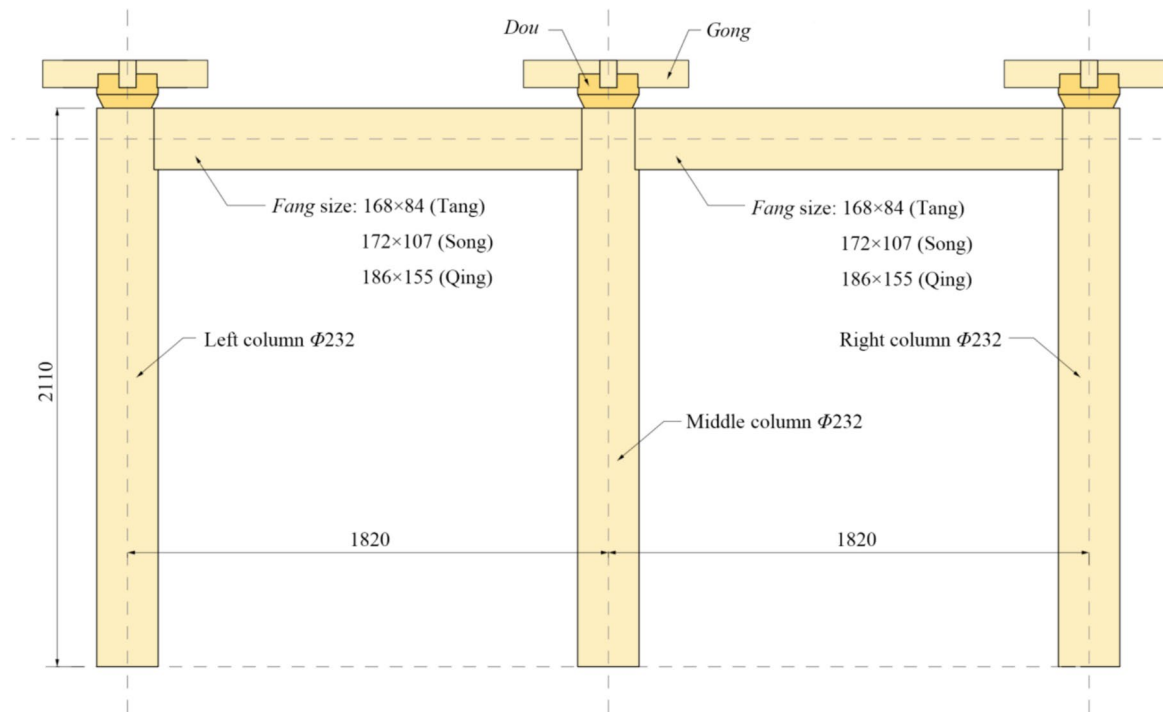
**Test program**

**Test model**

This study aims to investigate the influence of mortise–tenon joints on the lateral resistance of the timber frame. To reduce the influence of other structural factors on the experimental results, uniform-sized timber frames were used in the research. In the specimen design, the overall size, column height, column diameter, and general structural form of each timber frame were maintained uniformly. The impact of joint types on the lateral resistance of timber frames was examined by adjusting only the cross-sectional dimensions of beams and the types of mortise–tenon joints, ensuring the comparability of experimental results. Based on the height-to-diameter ratios of columns in typical timber buildings and relevant studies [20], the height-to-diameter ratio of columns in traditional Chinese timber buildings typically ranges from 8:1 to 10:1. The timber frames were designed to maintain this proportionate characteristic, with a column height of 2110 mm, a column diameter of 232 mm, and a span of 1820 mm between columns. As shown in Fig. 1, the models consist of columns and Fangs connected via mortise–tenon joints to form frames with three columns and two Fangs. Dou-Gongs are placed at the column heads to transmit loads. The cross-sectional dimensions of the Fangs and the types of mortise–tenon joints were designed with reference to examples from typical timber

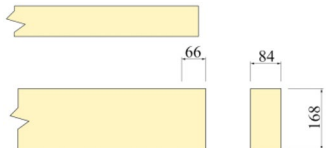
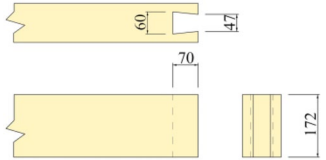
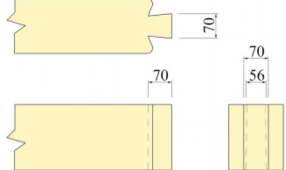
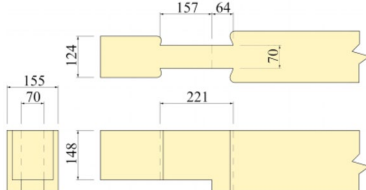
buildings, including the East Hall of Foguang Temple (Tang Dynasty), the Main Hall of Baoguo Temple (Song Dynasty), and the Forbidden City (Qing Dynasty). The Fang cross sections were proportionally scaled according to the actual dimensions in these reference examples, with the scaling factor determined by the ratio of the experimental model’s column diameter to that of the reference examples. The cross-sectional dimensions of the three Fangs are illustrated in Fig. 1. The dimensions of the mortise–tenon joints were determined based on traditional practices documented in *Traditional Techniques of Timber Construction in Ancient Chinese Architecture* [21] and *The Yingzao Fashi* [3]. The joint dimensions are provided in Table 1. The Dou had a diameter of 232 mm and a height of 151 mm, with Gong measuring 83×104×571 mm inserted in two directions. The models’ material was Chinese fir from Fujian (*Cunninghamia lanceolata* (Lamb.) Hook.), with a moisture content of 13.8%, an air-dry density of 0.37 g/cm<sup>3</sup>, and mechanical properties are shown in Table 2.

The three sets of mortise–tenon joints combinations are shown in Fig. 2a represents the *Zhi* mortise–tenon joints of the east hall of Foguang Temple in the Tang Dynasty, where the Fangs do not extend beyond the columns head, and their thickness remains unchanged at the intersection with the column head. (b) Represents the *Niekou gumao* mortise–tenon joints of Baoguo Temple in



**Fig. 1** Timber frame specimens (mm)

**Table 1** Sizes of mortise–tenon joints

Test model	Mortise–tenon joint type	Size (mm)
Tang	Zhi mortise–tenon joint	
Song	Niekou gumao mortise–tenon joint	
Qing	Yanwei mortise–tenon joint	
	Gutou mortise–tenon joint	

**Table 2** Mechanical properties of Chinese fir (MPa)

$E_L$	$E_R$	$E_T$	$f_L$	$f_R$	$f_T$
11959	1337	832	28.7	2.5	2.0

$E$  Compressive elastic modulus,  $f$  Compressive strength, L Longitudinal direction, R Radial direction, T Tangential direction

the Song Dynasty, where the *Fangs* do not extend beyond the columns head, and they are connected using a reverse dovetail structure. (c) Represents the conventional mortise–tenon joints of the Forbidden City in the Qing Dynasty, where one end of the *Fangs* extend beyond the columns head and are connected to the side columns using *Gutou* mortise–tenon joints. The other ends are connected to the middle columns using *Yanwei* mortise–tenon joints. Both types of mortise–tenon joints use the embracing shoulder style.

**Loading device and loading system**

The quasi-static test was conducted using a micro-computer controlled electro-hydraulic servo combined shear wall test system (YAW-250 J) supplied by Jinan Bangwei Instrument Co., Ltd. (Shandong, China). The horizontal hydraulic jack stroke range is  $\pm 250$  mm, and the maximum load is 250 kN. The vertical load ( $P$ ) was

applied by a movable vertical hydraulic jack to simulate the roof load. The vertical load was transferred from the steel beam to the distribution beam, which then disperses it to each column. Specifically, the middle column bore half of the load ( $P/2$ ), while each side column bore a quarter of the load ( $P/4$ ). The distribution beam was connected to the steel beam and the horizontal hydraulic jack using M24 high-strength bolts. The horizontal loading point was located 2400 mm away from the bottom of the column. The columns of the timber frame are directly placed on the base, simulating the floating pedestal connection characteristic of actual ancient Chinese timber buildings. Horizontal pushing was defined as the positive direction, while horizontal pulling was defined as the negative direction. The lateral displacement and restoring force of the timber frame were measured and output by the sensors located at the horizontal hydraulic jack of the shear wall test system. To measure the pull-out length and rotation angle of the mortise–tenon joints and column bases, 20 displacement gauges were set up in pairs, each positioned at mortise–tenon joints and column bases. The data from the displacement gauges were collected via a 30-channel TDS530 static data acquisition instrument. The rotation angle ( $\theta$ ) was determined by the ratio of

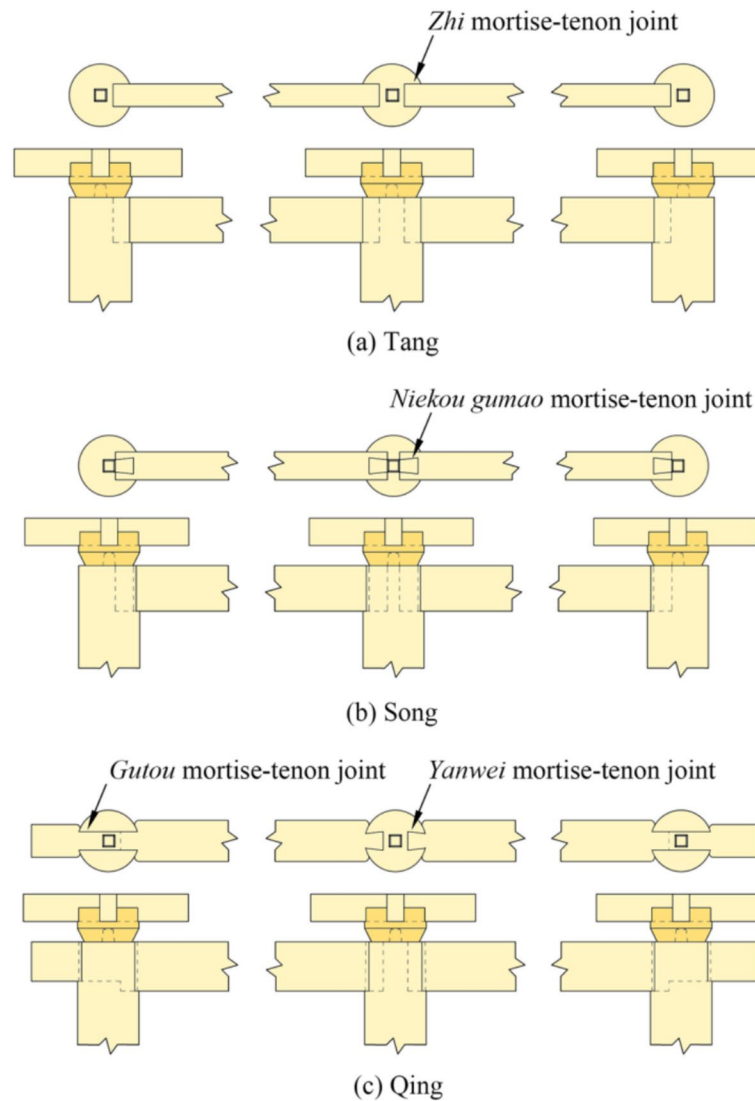


**Fig. 2** Three groups of mortise-tenon joints in timber frame specimens

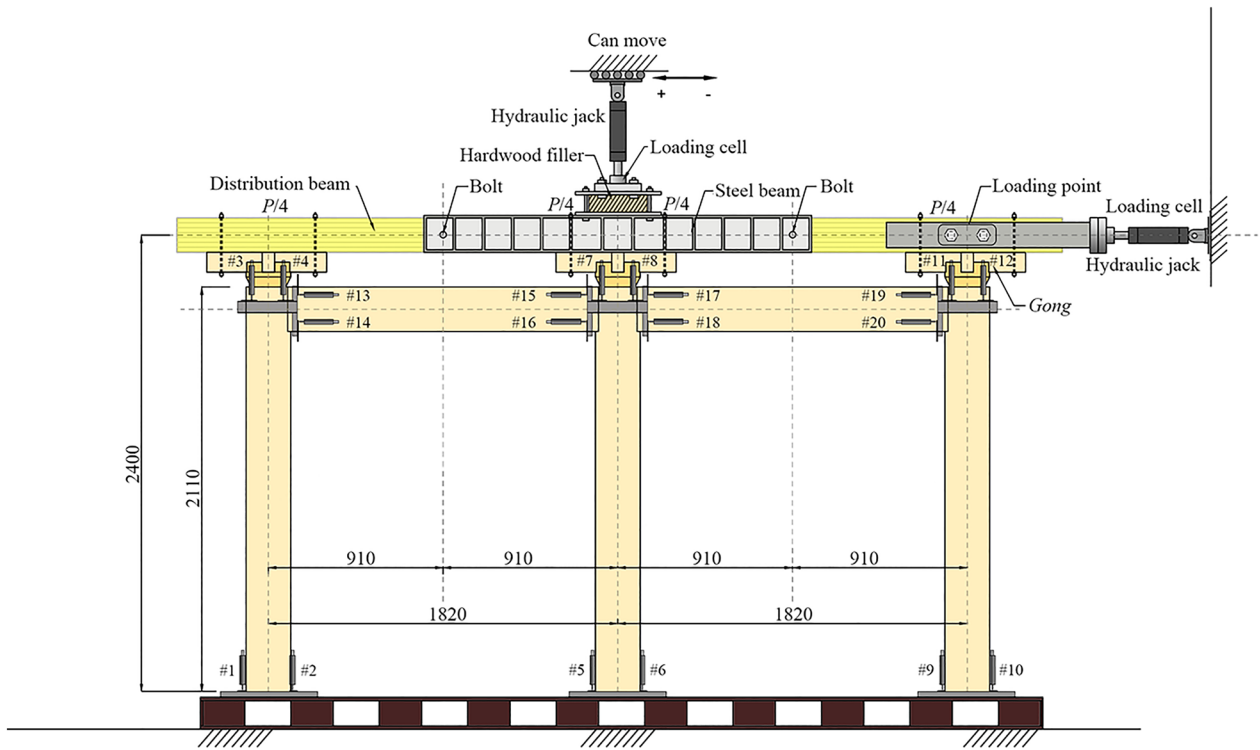
the difference in readings from each pair of displacement gauges to the perpendicular distance between the two gauges. These measurements were taken at the point of maximum displacement for each loading cycle. The pull-out length ( $\delta$ ) was defined as the relative displacement between the position of the *Fang's* centerline and the edge of the column. It was determined by the average of the readings from each pair of displacement gauges (measurements were taken once after completing a cycle). The experimental loading device and the arrangement of measuring points are shown in Fig. 3, where #*i* represents the displacement gauge number.

To quantify the restoring force components of the timber frame through the bending moment at the

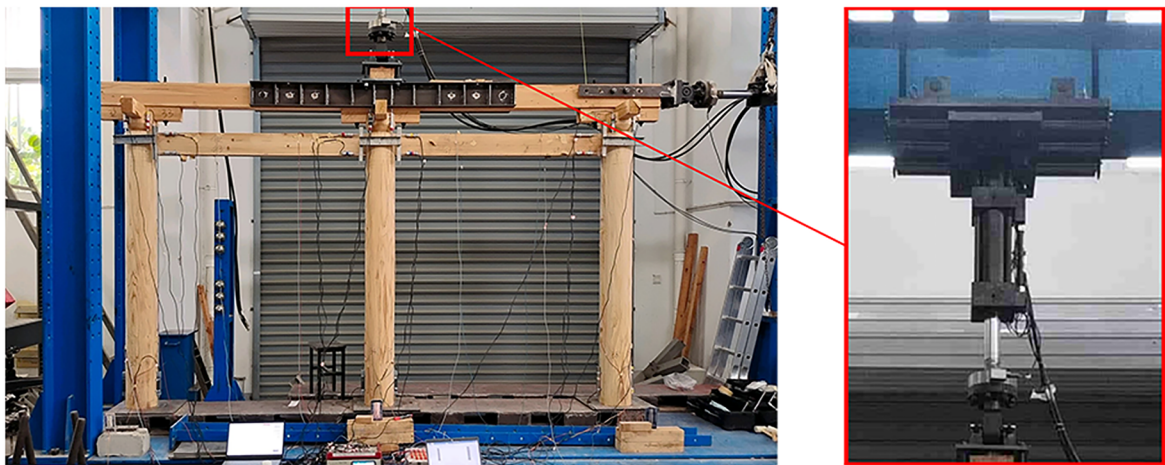
mortise-tenon joints, strain gauges were arranged in pairs at the positions indicated in Fig. 4. Strain data were acquired with a strain gauge box (DH3816N), with  $SG_i$  denoting the strain gauge number. The bending moment at the positions of the strain gauges was computed using Eq. 1. Figure 5 illustrates the method for calculating the bending moment at the mortise-tenon joints [22], while the calculation formulas for the joint moments  $M_1$  and  $M_2$  are provided in Eq. 2:

$$M = \sigma W = \frac{1}{2} \Delta \varepsilon E W \tag{1}$$

where  $\sigma$  is the strain,  $W$  is the section modulus in bending,  $\Delta \varepsilon$  is the strain difference,  $E$  is the modulus of elasticity:



(a) Diagram of the experimental loading device (mm)



(b) Test model

Fig. 3 Test model and device

$$M_i = \frac{M_3 - M_2}{x_3 - x_2} \left( x_i - \frac{x_2 + x_3}{2} \right) + \frac{x_2 - x_3}{2} \quad (2)$$

The meanings of the symbols in Eq. 2 are detailed in Fig. 5.

The calculation of the vertical load is based on the roof loads observed in the east hill of Foguang Temple, the

main hall of Baoguo Temple, and the Taihe Palace of Forbidden City. The load was calculated in proportion to the dimensions of the reference buildings and the test models. Upon calculating the average value, the vertical load was determined to be  $P=45$  kN.

The horizontal hydraulic jack was loaded according to the loading system shown in Table 3. The loading

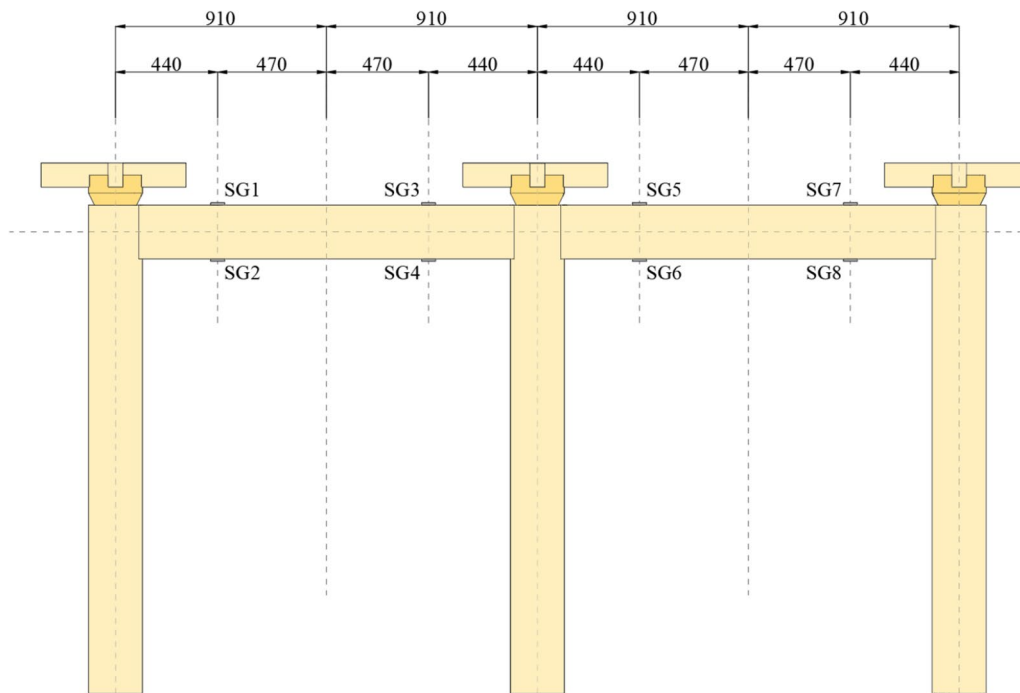


Fig. 4 Strain gauge position (mm)

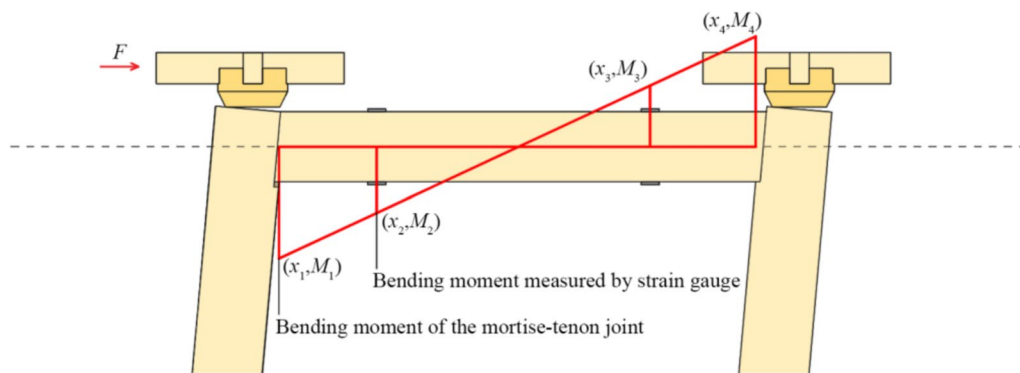


Fig. 5 Calculation method of mortise-tenon joint moment

Table 3 Quasi-static test loading system table

Cycle (No.)	Rotation angle (rad)	Displacement $\Delta$ (mm)
1	1/300	8
2	1/200	12
3	1/150	16
4	1/100	24
5	1/75	32
6	1/50	48
7	1/30	80
8	1/15	160

is controlled by horizontal displacement. The rotation angle in Table 3 is the rotation angle of the timber frame corresponding to the displacement. The loading refers to the loading system of wood frame shear wall [23] and existing research [24]. Positive and negative loading are performed once per cycle. The three timber frame tests are, respectively, abbreviated as T-F, S-F, and Q-F for convenience. In this context, the letters T, S, and Q represent the Tang, Song, and Qing dynasties, respectively, while F denotes frame.

## Results and discussion

### Experimental phenomena

From the experimental tests, the deformations observed during the loading process were similar among the three test frames, and the components in the frames did not fail. There was no obvious slippage at the column bases, and the deformations of the frames were basically restored after unloading. This was due to the column bases being disconnected from the foundation, the semi-rigid characteristics of mortise–tenon joints, and the material properties of the wood.

Figure 6 shows the deformation of the frame when the horizontal loading displacement is  $-160$  mm. At this point, one side of column base was uplifted (Fig. 6g).

The tenons were pulled out, forming a triangular-shaped extracted portion. When the *Fangs* positioned on the loading direction side of the column (to the right during negative loading), the extracted portion of the tenon forms an upright triangle (Fig. 6a *Zhi* mortise–tenon joint on the left column, Fig. 6b *Niekou gumao* mortise–tenon joint on the left column, Fig. 6c *Gutou* mortise–tenon joint on the left column); conversely, it forms an inverted triangle (Fig. 6d *Zhi* mortise–tenon joint on the middle column, Fig. 6e *Niekou gumao* mortise–tenon joint on the middle column, Fig. 6f *Yanwei* mortise–tenon joint on the middle column). Although the pull out occurred in four types of mortise–tenon joint at the maximum loading displacement, the pull-out lengths

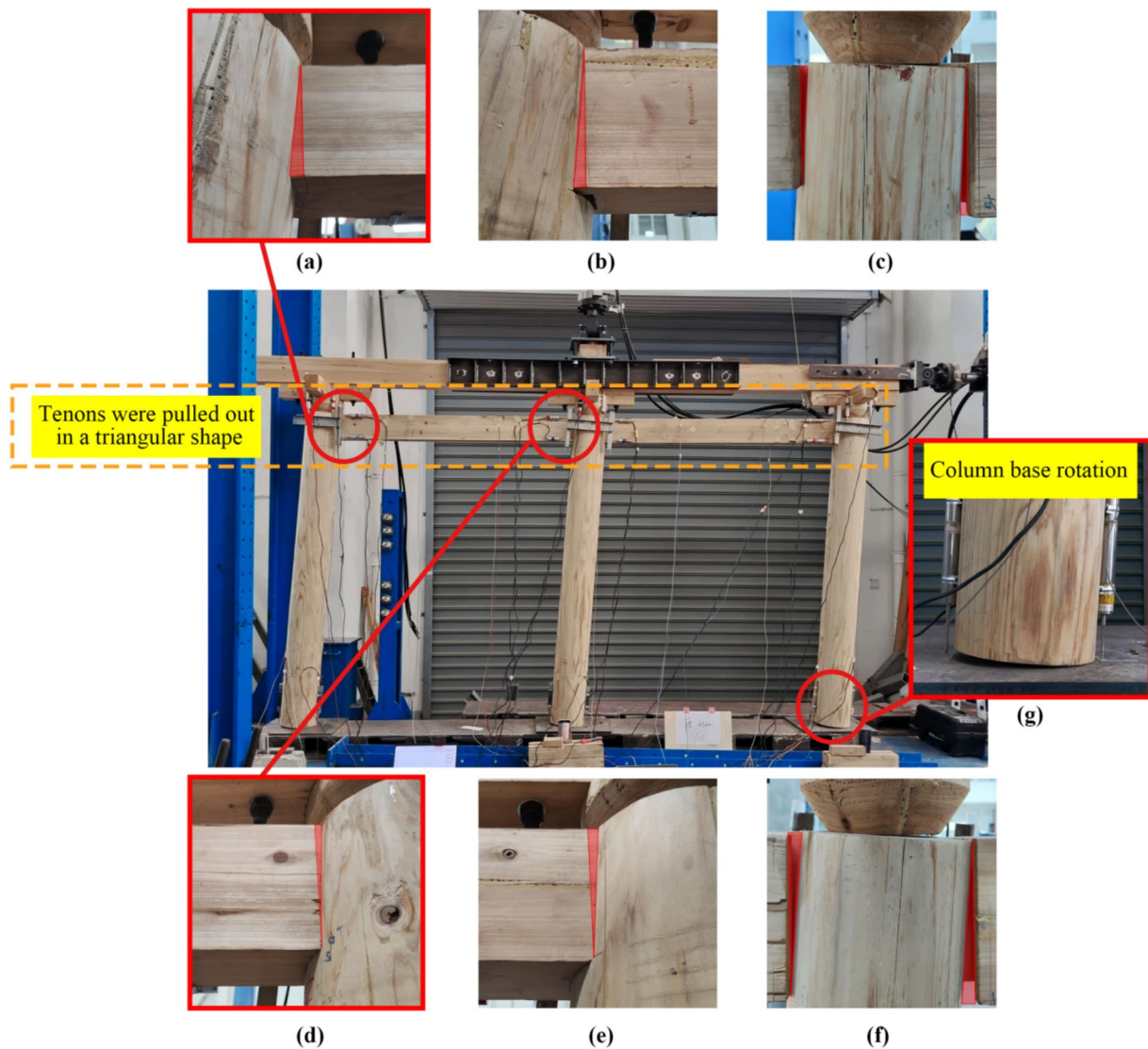


**Fig. 6** Deformation of the frame, joints, and column bases



were small, and the joints did not fail. It indicates that the mortise–tenon joints can withstand significant horizontal lateral displacement in timber frames.

After tests, noticeable compression deformation appeared on the lower surface of the tenon (Fig. 7), while the compression deformation on the mortise of the

column was smaller (Fig. 8). Due to the embracing shoulder design of the mortise–tenon joints in Qing frame, compression deformation can be observed at the contact area between the column surface and the tenon shoulder, which is attributed to the higher compressive strength of wood in the longitudinal direction.

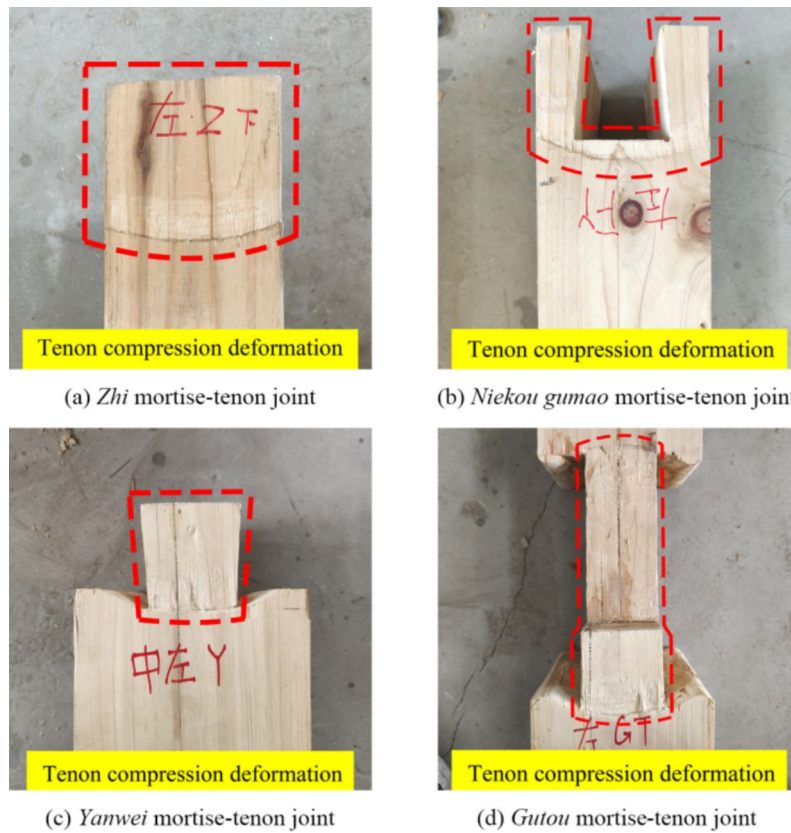


**Fig. 7** Compression deformation on the lower surface of the tenon after tests

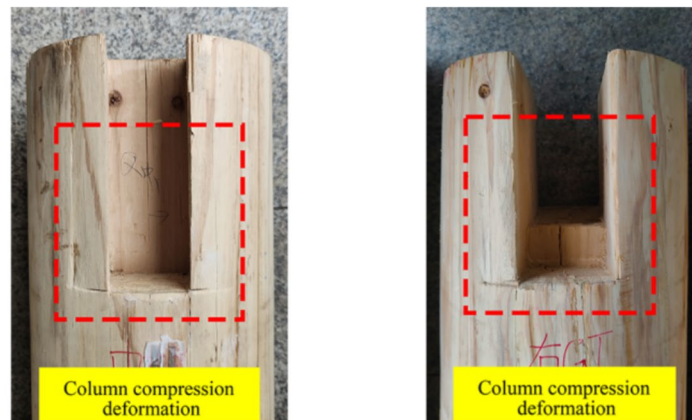


**Fig. 8** Compression deformation of Qing frame columns after tests

Based on the test results, there is no significant difference in the column base rotation angles among the three frames. The rotation direction is defined as positive when the angle between the *Fang* at the mortise–tenon joint and the column decreases (Fig. 9). Figure 10 illustrates the relationship between the mortise–tenon joint rotation at different positions and the overall timber frame rotation. Overall, the type of mortise–tenon joint has a minor effect on the rotation angles. The four types of mortise–tenon joints exhibit similar trends in rotation

angles. The mortise–tenon joint rotation angles and the timber frame rotation angles exhibit a linear relationship. Although the differences are minor, the slopes of the fitted curves for the joint rotation angles relative to the timber frame rotation angles show the following order: *Zhi* mortise–tenon joint > *Niekou gumao* mortise–tenon joint > *Yanwei* mortise–tenon joint > *Gutou* mortise–tenon joint. The stronger the deformation resistance of the mortise–tenon construction, the more it limits joint rotation. Consequently, the slope can indicate

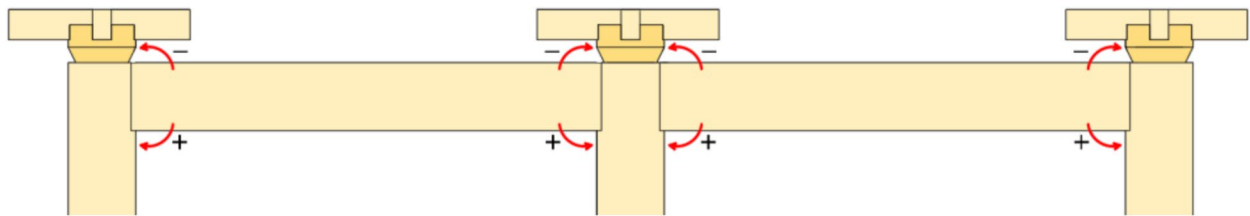


Fig. 9 Illustration of mortise–tenon joint rotation direction

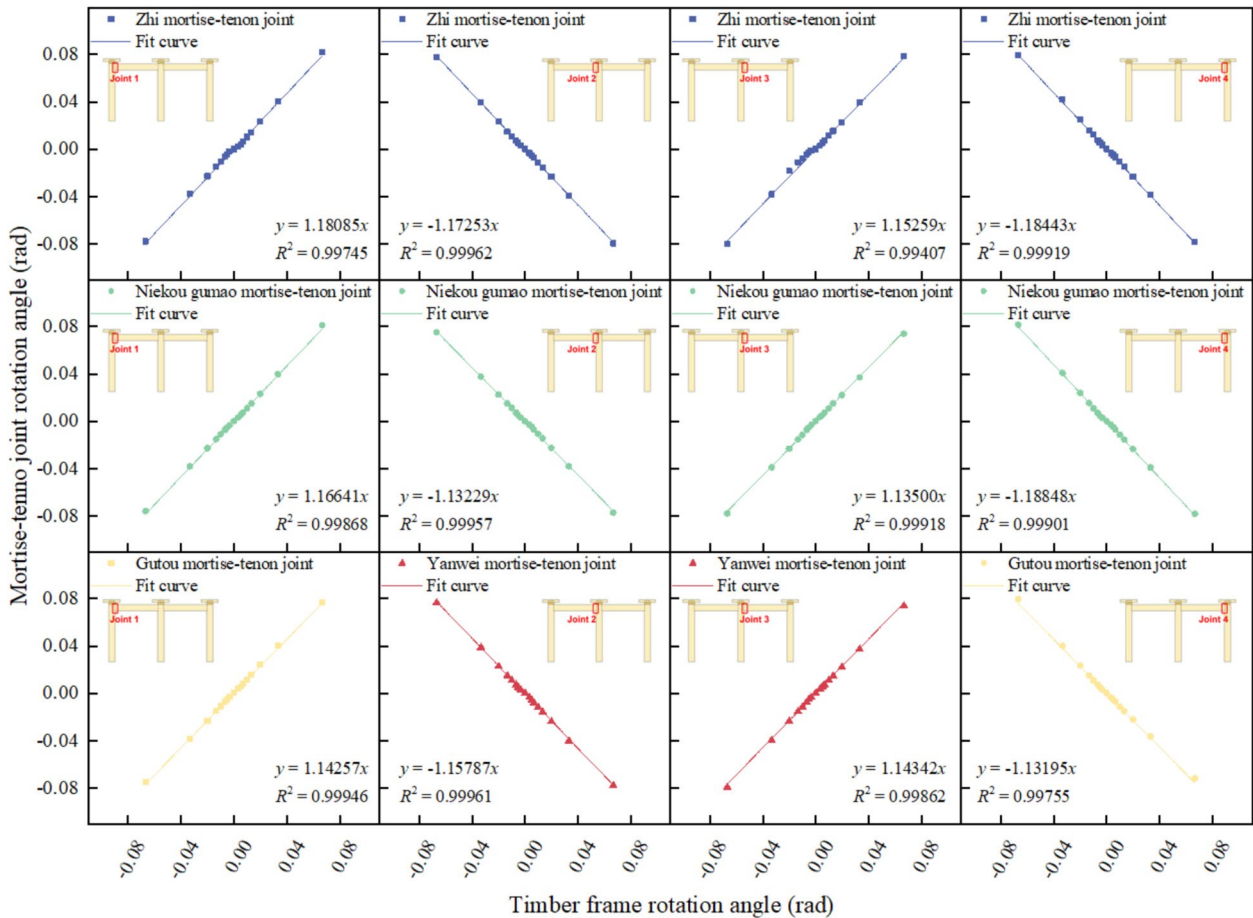


Fig. 10 Relationship between the mortise–tenon joint rotation and the overall timber frame rotation

the deformation resistance capacity of mortise–tenon joints. A reduced slope signifies enhanced resistance to deformation.

The pull-out behavior of each mortise–tenon joint is shown in Fig. 11. Among the different types of joints, the *Gutou* mortise–tenon joint has good resistance to pull out and effective reset performance. The *Yanwei* mortise–tenon joint located at joint 3 has a greater pull-out length due to the large gap that exists between the mortise–tenon joints, whereas the *Yanwei* mortise–tenon joint at joint 2 exhibits better resistance to pull out than the *Zhi* mortise–tenon joint. Comparing the *Zhi* mortise–tenon joints and *Niekou gumao* mortise–tenon joints at the four joint positions, it is found that as the horizontal loading displacement increases, the *Niekou gumao* mortise–tenon joints exhibit gradually superior resistance to pull out compared to the *Zhi* mortise–tenon joints. This is attributed to the reverse dovetail structure within the *Niekou gumao* mortise–tenon joints. In addition, in some cases, a negative pull-out length was observed at certain joints (Fig. 11c, d), which is caused by the initial gaps among components gradually disappearing due to compression during the loading process. From Fig. 11e, at the end of the experiment, the pull-out length of each joint does not exceed 5 mm, indicating that the timber frames have good deformation recovery capability.

#### Hysteresis curve and envelop curve

The hysteresis curves and envelope curves obtained from the three experiments are shown in Fig. 12. The hysteresis curves of the three timber frames all exhibit a swinging structure characteristic with full ends and pinched middles. From the hysteresis curves of the three timber frames, the curve of the subsequent loading cycle basically follows the trajectory of the previous cycle. This indicates that the load-bearing capacity of the timber frames does not show a significant decline, suggesting minimal damage to the components. This demonstrates that such structures maintain good resistance to damage and load-bearing capacity under seismic forces. The restoring force rapidly decreases at the beginning of the unloading phase in each cycle, and the greater the horizontal loading displacement and the greater the compression deformation of the components, the more the restoring force decreases. Meanwhile, the larger the horizontal loading displacement, the smaller the overall restoring force in the unloading phase. This means that with increasing horizontal loading displacement, the structure experiences more frictional sliding and plastic deformation.

The fullness of the hysteresis curves of the three timber frames varies (Fig. 12a–c). The hysteresis curve of the

Q–F is significantly fuller than it of the T–F and S–F. This is due to the *Gutou* structure and the embracing shoulder style causing higher restoring force and more compressive friction in the later stages of loading, thereby absorbing more energy. However, excessive compressive friction also leads to a weakening of deformation recovery capability. From the hysteresis curves of the three timber frames, it can be seen that the Q–F exhibits the largest residual deformation, followed by the S–F.

The envelope curves of the three timber frames are all antisymmetric (Fig. 12d), but their trends are significantly different. The maximum restoring force of the T–F appears at a horizontal loading displacement of around 32 mm. After that, its restoring force gradually decreases as the horizontal loading displacement increases. For the S–F, the restoring force stops increasing and remains constant when the horizontal loading displacement reaches 62 mm. The restoring force of the Q–F exhibited two stages of increase, reaching its maximum at a horizontal loading displacement of 160 mm. The peak restoring force of the Q–F is 1.76 times that of the T–F and 2.04 times that of the S–F. A quantitative analysis was performed to examine the factors contributing to these differences, focusing on the bending moment of mortise–tenon joints and the overall restoring force of timber frames. The restoring force of timber frames is primarily provided by the rocking of columns and the rotation of mortise–tenon joints (Fig. 13). As illustrated in Fig. 14, the column rocks under the horizontal force  $F$ , resulting in a column top displacement  $\delta_c$ . When  $\delta_c$  is smaller than the column diameter, the rocking column provides a resisting moment  $M_c$ , due to the vertical load  $P_c$ . In this case, the rocking column contributes positively to the restoring force of the timber frame. However, when  $\delta_c$  exceeds the column diameter, the rocking of the column may cause structural collapse, resulting in a negative effect on the restoring force. Since deformation occurs during column rocking, altering the point of resultant force application, the actual restoring force of the rocking column follows a curve that initially rises and then declines [25]. The moment equilibrium relationship of the timber frame is expressed in Eq. 3. The sum of the column top moment  $M_{tc}$  and column bottom moment  $M_{bc}$  represents the total moment  $M_c$ , produced by the rocking column. The restoring force contributed by the rocking column  $F_c$  is calculated as  $M_c/H$ , while the restoring force provided by the mortise–tenon joints  $F_b$  is calculated as  $M_b/H$ . To eliminate discrepancies caused by installation and material variations, the restoring forces under positive and negative loading directions were averaged:

$$FH = M_{tc} + M_{bc} + M_b = M_c + M_b \quad (3)$$

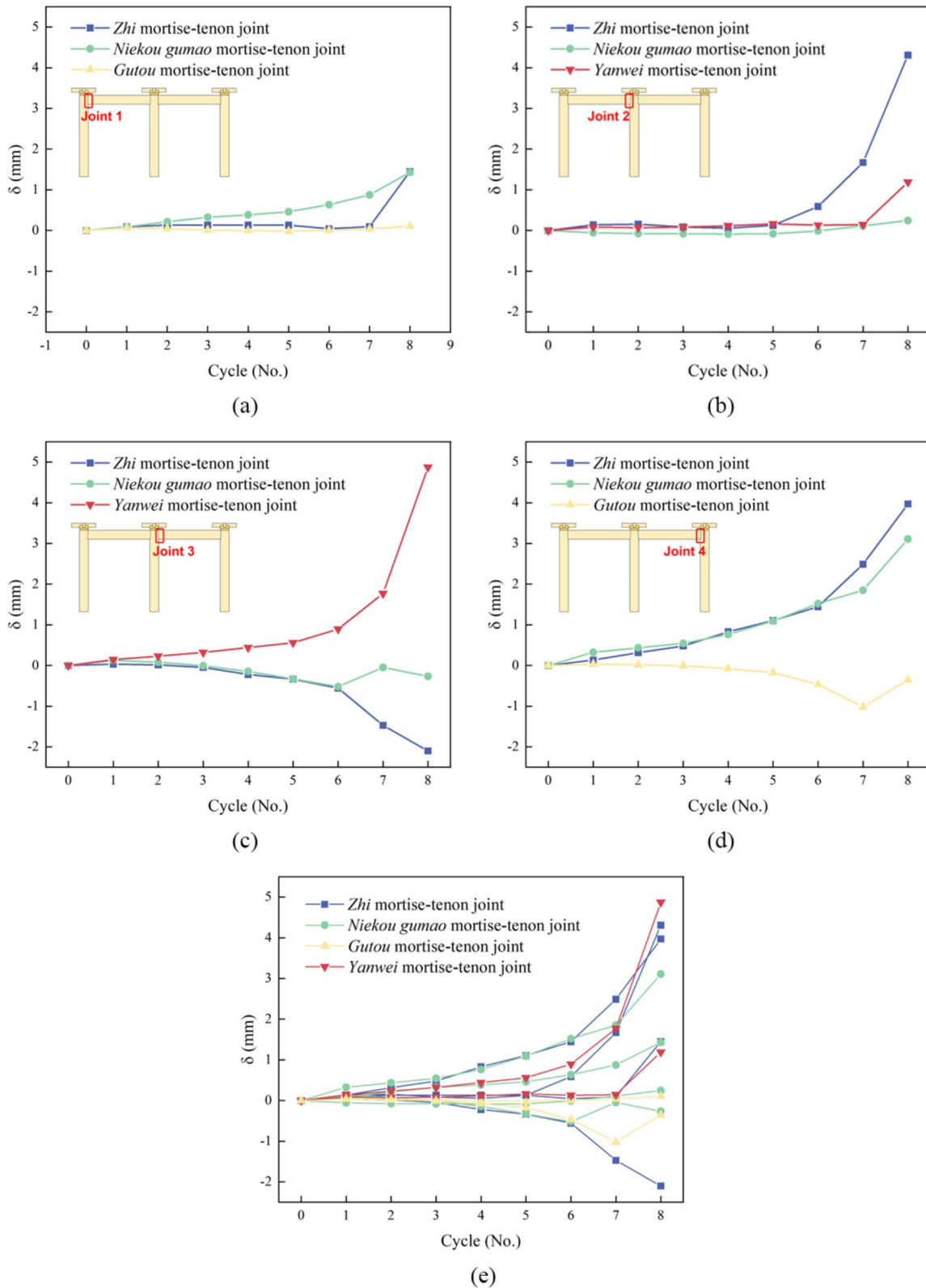
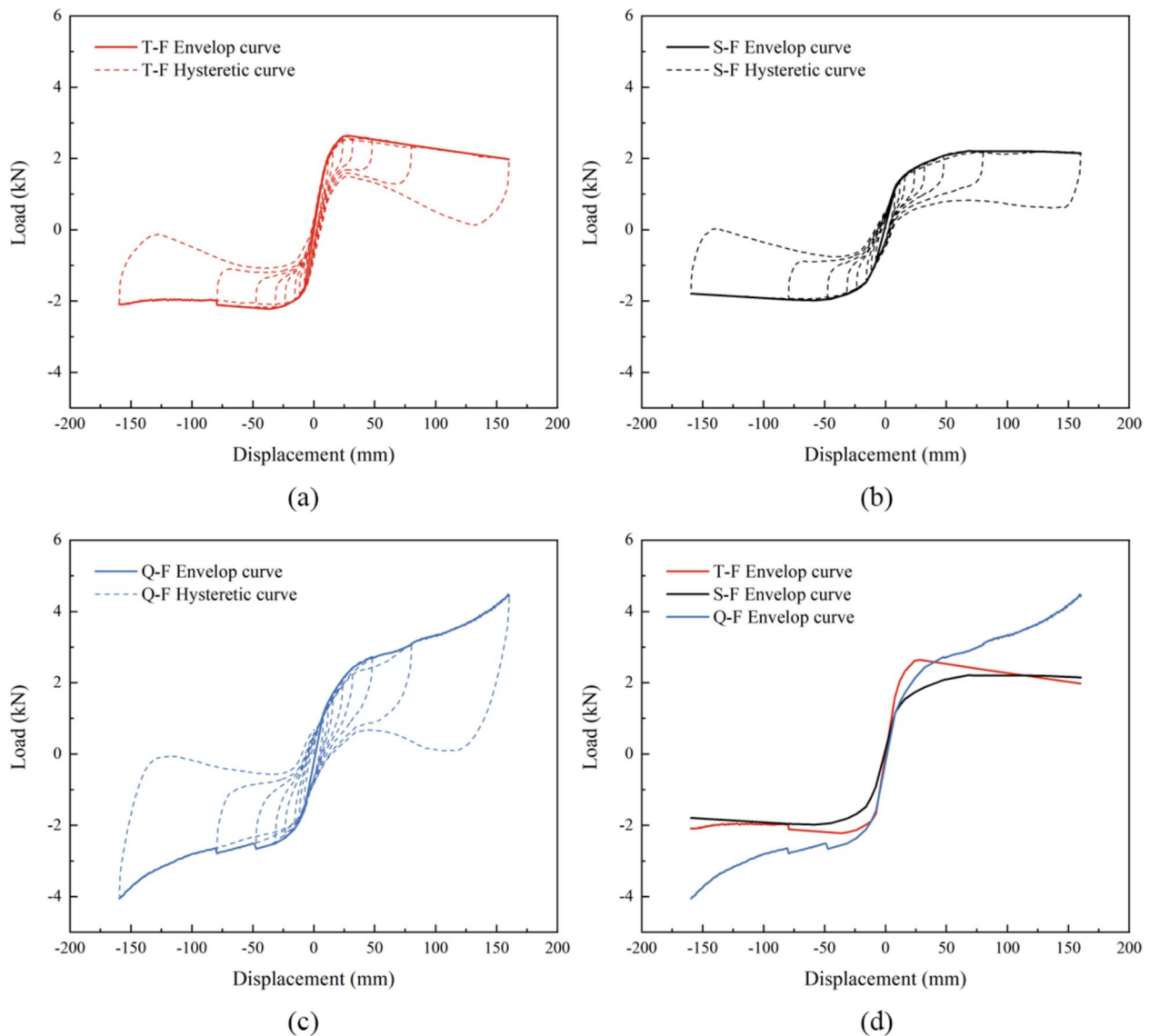


Fig. 11 Pull-out length of the mortise-tenon joints at different positions



**Fig. 12** Hysteresis curves and envelop curves

The components of the restoring force for the three timber frames are illustrated in Fig. 15. In all three frames, the restoring force curves of the rocking columns demonstrate the previously noted pattern of initial rise followed by a decline. At minimal horizontal loading displacements, the rocking columns are the primary contributors to the restoring force. As the horizontal loading displacement increases, the positive effect of the rocking columns declines leading to a reduction in their restoring force and contribution ratio. Simultaneously, the rotation of the mortise–tenon joints increases, resulting in variations in the restoring force. As the joint rotation angle increases, the reverse dovetail structure within the *Niekou gumao*

mortise–tenon joint begins to compress, resulting in higher restoring force and better deformation resistance compared to the *Zhi* mortise–tenon joint. The restoring force of the Q–F exhibited two stages of increase. During the initial stage, when the horizontal loading displacement is relatively small, the restoring force is primarily provided by the rotation of the columns. As the horizontal loading displacement increases, the compression of the mortise–tenon joints intensifies, resulting in an increase in the restoring force generated by these joints, while the restoring force provided by the columns decreases. Consequently, the mortise–tenon joints become the dominant source of restoring force. Under the strong binding effect of the

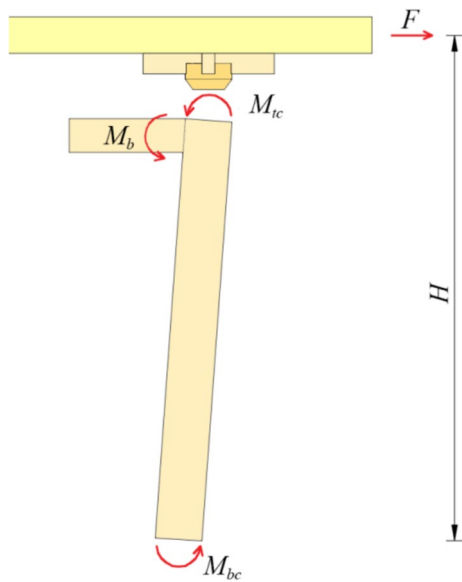


Fig. 13 Moment equilibrium in the timber frame

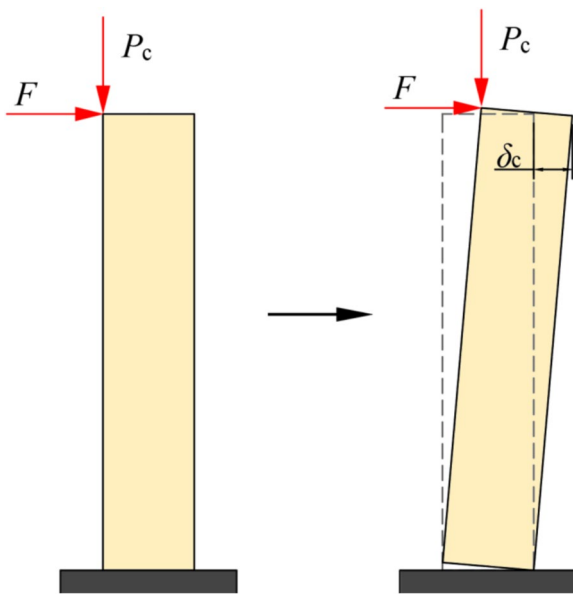


Fig. 14 Schematic diagram of rocking column

Gutou mortise–tenon joints, the frame’s restoring force experiences a second stage of increase. Moreover, the strong binding effect of the Q–F significantly increases its maximum restoring force. This is partly because the Gutou mortise–tenon joint restricts further rotation of the columns, and partly because the Q–F uses embracing shoulder style mortise–tenon joints, where the tenon shoulder compresses against the column, which could also be found in Fig. 8.

The restoring force contribution ratio is defined as the percentage of the restoring force produced by the columns or mortise–tenon joints in relation to the overall restoring force of the timber frame. Figure 16 illustrates the ratio of restoring force contribution between columns and mortise–tenon joints. During the initial loading stage (horizontal displacement of 8 mm), the contribution ratios of the restoring force from the rocking columns in the T–F, S–F, and Q–F frames were 96.91%, 92.24%, and 82.45%, respectively. At this stage, the mortise–tenon joints in the T–F and S–F frames made a minimal impact, but the joints in the Q–F frame, due to their stronger resistance to deformation, were able to provide a certain amount of restoring force even at the beginning. As the horizontal loading displacement increased, the contribution ratio of the restoring force from the mortise–tenon joints increased. The stronger their capacity for resistance to deformation, the more significant increase in their contribution ratio. At a loading displacement of 160 mm, the contribution ratios of the restoring force provided by the mortise–tenon joints in the T–F, S–F, and Q–F frames were 37.41%, 64.26%, and 87.17%, respectively.

**Stiffness**

The stiffness for the three test frames were calculated according to Eq. 4 [26]. The stiffness degradation curves for the three frames are shown in Fig. 17:

$$K_i = \frac{|+F_i| + |-F_i|}{|+X_i| + |-X_i|} \tag{4}$$

where  $+F_i$  and  $-F_i$  are the peak loads in the positive and negative directions for the  $i$ -th cycle, respectively,  $+X_i$  and  $-X_i$  are the displacement values corresponding to the peak loads in the positive and negative directions for the  $i$ -th cycle, respectively.

The stiffness in the three tests rapidly decreased during the first five loading cycles (horizontal loading displacement  $\leq 32$  mm). This can be explained by that at the initial stage of small horizontal loading displacement, the rotational stiffness of the columns plays a decisive role in the overall stiffness of the timber frame. In the previous research conducted by Wu et al. of the mechanical behavior of single columns [27], it was also shown that the initial rotation stage exhibits significant stiffness degradation of the columns. During this period, the static compression constitutive relationship of the wood in the perpendicular grain direction is in a weak linear hardening state, and the mortise–tenon joints and other areas under perpendicular grain compression rapidly develop plastic deformation. When the horizontal loading displacement is large, the rotation angles of the mortise–tenon joints increase, and

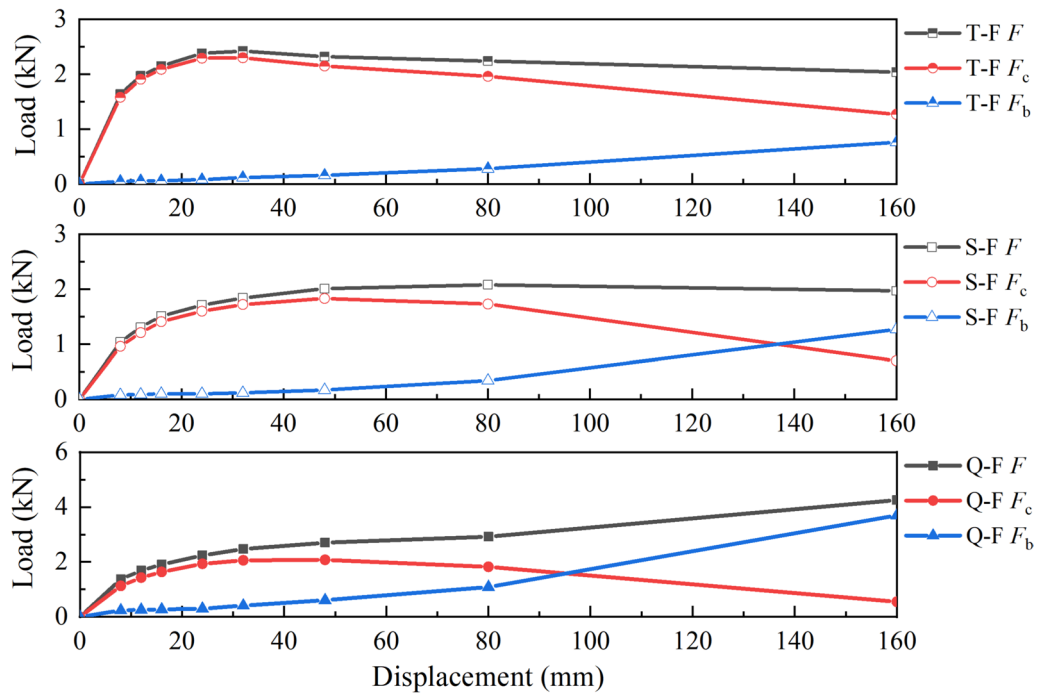


Fig. 15 Contributions from columns and mortise-tenon joints

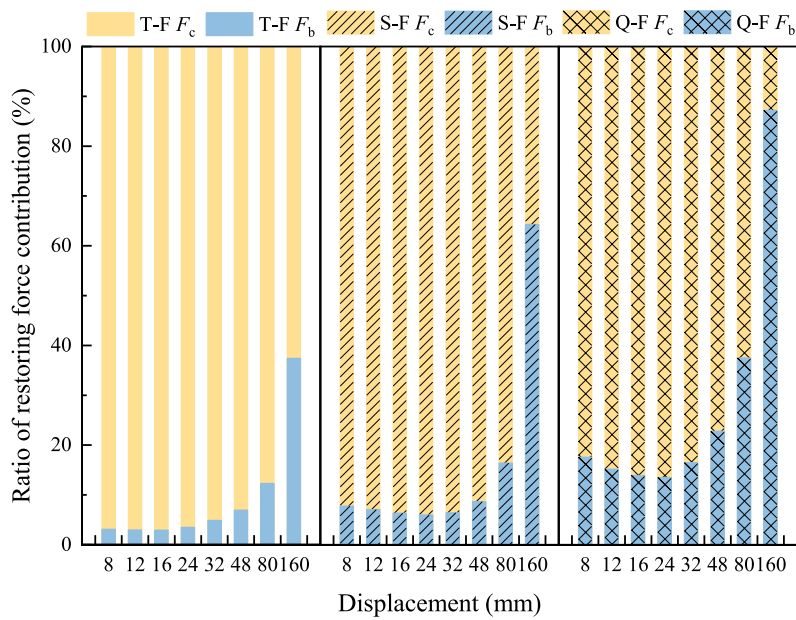


Fig. 16 Ratio of restoring force contribution between columns and mortise-tenon joints

the binding effect becomes more pronounced, which slows down the degradation of the overall stiffness of the frame. Subsequently, as the wood becomes more compressed and densified, it enters a significant hardening stage [28]. The force required to produce plastic

deformation increases rapidly, and the rate of stiffness degradation gradually slows down.

The stiffness of the T-F slightly increases after the 6th loading cycle (horizontal loading displacement  $\geq 48$  mm). This is mainly due to the gradual disappearance of some

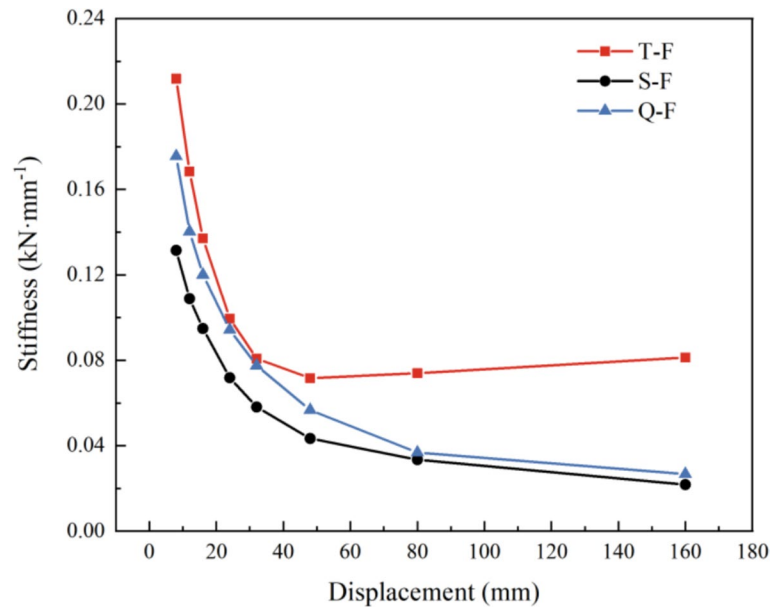


Fig. 17 Stiffness degradation curves

initial gaps between components [15]. This phenomenon is related to the tenon squeezing into the mortise at joint 3 (Fig. 11c). The same phenomenon also occurs in the S–F, but since the degree of the tenon squeezing into the mortise is less than that in the T–F (Fig. 11b, c), the rate of stiffness degradation in the S–F remains essentially unchanged after the 6th cycle (horizontal loading displacement  $\geq 48$  mm). The Yanwei mortise–tenon joints and Gutou mortise–tenon joints used in the Q–F experience more compressive deformation, accelerating the stiffness degradation of the frame. However, when the horizontal loading displacement is large, the strong binding effect of the Gutou mortise–tenon joints

significantly mitigates the stiffness degradation of the frame. Therefore, the stiffness of the Q–F degrades rapidly before the 7th loading cycle (horizontal loading displacement  $\leq 80$  mm). After this point, the rate of stiffness degradation significantly slows down.

### Energy dissipation

The equivalent viscous damping coefficient  $\xi_{eq}$  of the frame were calculated using Eq. 5 [26] to evaluate the energy dissipation capacity of the frames. The calculation results are shown in Fig. 18a, and the energy dissipation for each cycle of the three frames is shown in Fig. 18b:

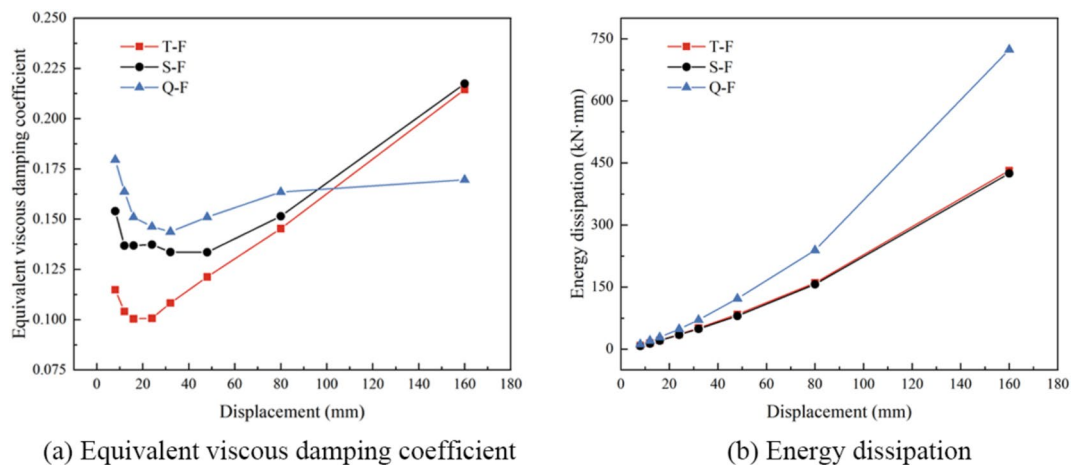


Fig. 18 Energy dissipation curve



$$\xi_{eq} = \frac{1}{2\pi} \cdot \frac{S_{loop}}{S_E} \tag{5}$$

where  $S_{loop}$  is the area enclosed by the hysteresis curve, representing the energy dissipated by the frame during one loading cycle;  $S_E$  is the energy absorbed by an elastomer when it reaches the same displacement.

From the variation pattern of  $\xi_{eq}$  in Fig. 18a, the energy dissipation capacity of the three timber frames shows a declining trend during the initial loading cycles. This is partly due to the gradual disappearance of initial gaps in the frames caused by frictional sliding, and partly because the frames are still in the elastic deformation stage, with small residual deformations and not full hysteresis loops. As the horizontal loading displacement increases, the compressive deformation and frictional sliding between components also increase. The energy dissipation capacity of each frame starts to show a significant improvement at different loading cycles. In addition, the extent of the increase in energy dissipation capacity for the three timber frames is related to the slip resistance of the mortise–tenon joints used, the stronger the slip resistance, the slower the increase in energy dissipation capacity.

As shown in Fig. 18b, the energy dissipation and its growth rate for the three timber frames increase with the horizontal loading displacement. It is noteworthy that the energy dissipation values for the T–F and S–F are very similar, but the reasons for their energy dissipation are not entirely the same. The T–F has a higher

maximum restoring force, while the S–F has a stronger ability to limit deformation and a fuller hysteresis loop. The energy dissipation of the Q–F is significantly higher than that of the other two types of frames, and the difference increases with the horizontal loading displacement. This is because, in the later stages of loading, the embracing shoulder style *Gutou* mortise–tenon joints and the *Yanwei* mortise–tenon joints in the Q–F frame generate higher restoring forces and more plastic deformation, thereby increasing the energy dissipation of the frame.

### Restoring force model

To reflect the hysteresis characteristics of the frames and to characterize its restoring force features, a restoring force model was established with reference to the research of several scholars [18, 29, 30]. To eliminate the asymmetry in the hysteresis curves caused by material anisotropy and other factors, the characteristic parameters were taken as the average of the test results for both positive and negative loading directions. All three frames use a four-linear restoring force model, with T–F and S–F models in Fig. 19 and Q–F model in Fig. 20. It is important to note that, except for the method of determining the position of point C, Figs. 19 and 20 represent the same restoring force model. The restoring force model is applicable to timber frames with mortise–tenon joint connections between columns and *Fangs*.

As shown in Fig. 19, the envelope curve is simplified into a four-linear model: elastic stage OA, first yield stage

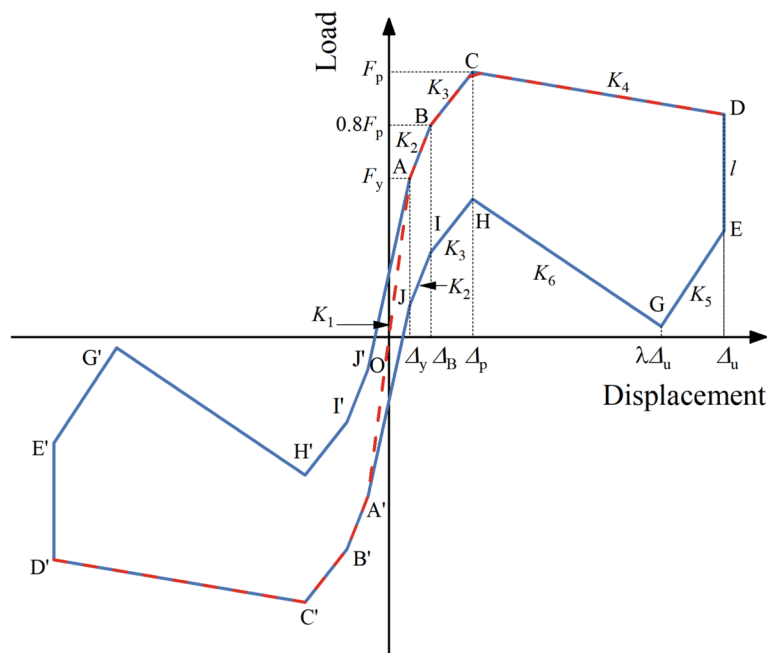


Fig. 19 Restoring force models for T–F and S–F

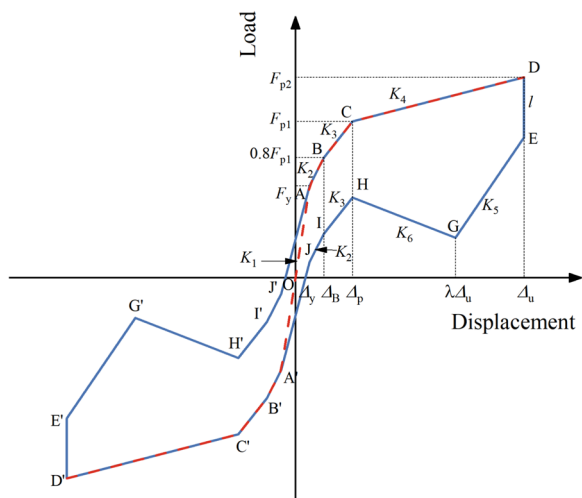


Fig. 20 Restoring force models for Q-F

AB, second yield stage BC, and descending stage CD. The occurrence of two yield stages may be due to the combined effects of the mortise–tenon joints and the rocking columns. As shown in Fig. 20, the Q–F does not exhibit a peak load point during the mid-stage of horizontal loading due to the influence of the *Gutou* mortise–tenon joints. From the results of the T–F and S–F, it is found that the peak load point in the mid-stage of loading is similar in horizontal loading displacement to the peak load point in the mid-stage of unloading (points C and H in Fig. 19). Thus, the peak load point C during the mid-stage of horizontal loading for the Q–F is determined.  $K_1$

is the initial stiffness, while  $K_2$ ,  $K_3$ , and  $K_4$  are the secant stiffnesses for their respective stages.

The stiffness degradation of the unloading branch in the restoring force model is depicted in Fig. 21. The following scenarios are considered:

- (1) When  $d \leq |\Delta_y|$ . The element remains in the elastic stage without any plastic deformation or damage. Stiffness degradation is not considered during unloading. Loading follows path OA and unloading retraces the original path.
- (2) When  $|\Delta_y| \leq d \leq |\Delta_B|$ . The loading stiffness degrades to  $K_2$ . At the start of unloading, due to an abrupt recovery, the path first follows a near-vertical segment of length  $l$  to point E (horizontal loading displacement =  $\Delta_u$ ). Then, unloading continues with stiffness  $K_2$  to point J (horizontal loading displacement =  $\Delta_y$ ), followed by reverse loading toward point A'.
- (3) When  $|\Delta_B| \leq d \leq |\Delta_P|$  and  $|\lambda\Delta_u| \leq |\Delta_B|$ . The loading stiffness further degrades to  $K_3$ . During unloading, the curve initially follows segment DE to point E (horizontal loading displacement =  $\Delta_u$ ), then unloads with stiffness  $K_5$  to point G (horizontal loading displacement =  $\lambda\Delta_u$ ), continues with stiffness  $K_2$  to point J (horizontal loading displacement =  $\Delta_y$ ), and finally reverses loading toward A'.
- (4) When  $|\Delta_B| \leq d \leq |\Delta_P|$  and  $|\lambda\Delta_u| > |\Delta_B|$ . The loading stiffness remains  $K_3$ , and the unloading curve consists of five segments. It initially unloads along DE to point E (horizontal loading displacement =  $\Delta_u$ ),

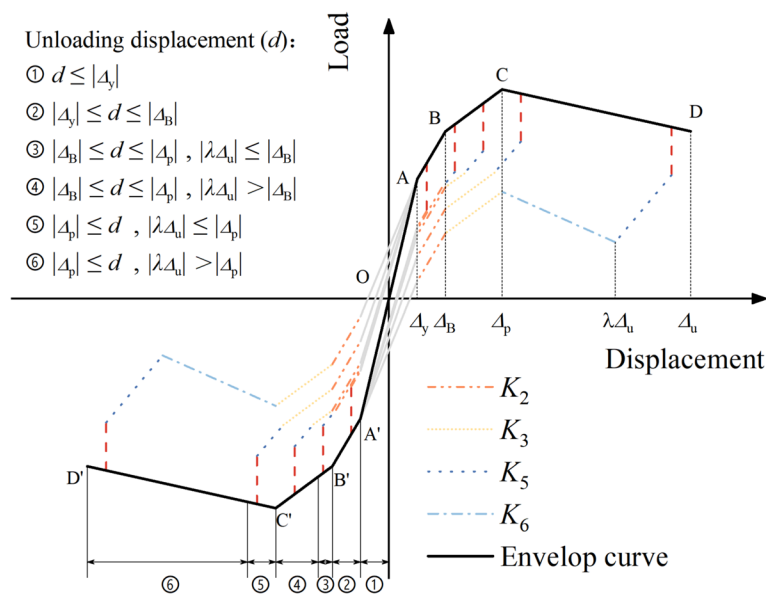


Fig. 21 Stiffness degradation of the unloading branch

then with stiffness  $K_5$  to point G (horizontal loading displacement =  $\lambda\Delta_u$ ), further with stiffness  $K_3$  to point I (horizontal loading displacement =  $\Delta_B$ ), then with stiffness  $K_2$  to point J (horizontal loading displacement =  $\Delta_y$ ), and finally reverses loading toward A'.

- (5) When  $|\Delta_p| \leq d$  and  $|\lambda\Delta_u| \leq |\Delta_p|$ . The loading stiffness degrades to  $K_4$ . The unloading curve follows the same pattern as the case  $|\Delta_B| \leq d \leq |\Delta_p|$  and  $|\lambda\Delta_u| > |\Delta_B|$ .
- (6) When  $|\Delta_p| \leq d$  and  $|\lambda\Delta_u| > |\Delta_p|$ . The loading stiffness degrades to  $K_4$ , and the unloading curve consists of six segments. The curve initially unloads along DE to point E (horizontal loading displacement =  $\Delta_u$ ), then with stiffness  $K_5$  to point G (horizontal loading displacement =  $\lambda\Delta_u$ ). Subsequently, the unloading stiffness changes to  $K_6$ . As the frame unloads, the horizontal loading displacement decreases, the positive effect of the rocking column enhances, causing the restoring force to rise toward point H (horizontal loading displacement =  $\Delta_p$ ). Unloading then continues with stiffness  $K_3$  to point I (horizontal loading displacement =  $\Delta_B$ ), further with stiffness  $K_2$  to point J (horizontal loading displacement =  $\Delta_y$ ), and finally reverses loading toward A'.

The characteristic stiffness and coefficients for each stage of three frames are determined based on the results of three tests (Table 4), with  $K_5$  and  $K_6$  fitted from the experimental results. The coordinates of each point (points E, G, H, I, and J) of the unloading branch are determined from Eqs. (6)–(10):

$$X_E = \Delta_u, Y_E = Y_D - l \tag{6}$$

$$X_G = \lambda\Delta_u, Y_G = K_5(X_G - X_E) + Y_E \tag{7}$$

$$X_H = \Delta_p, Y_H = K_6(X_H - X_G) + Y_G \tag{8}$$

$$X_I = \Delta_B, Y_I = K_3(X_I - X_H) + Y_H \tag{9}$$

$$X_J = \Delta_y, Y_J = K_2(X_J - X_I) + Y_I \tag{10}$$

The comparison between the test results and the calculation results of the restoring force model for the three frames are shown in Fig. 22. It can be observed that the calculated restoring force curves fit the test results well, accurately reflecting the restoring force characteristics and stiffness changes of the frames at various stages during both loading and unloading processes. Moreover, this model effectively reflects the restoring force of timber frames using different types of mortise–tenon joints.

**Table 4** Characteristic parameters of the restoring force model

Test	Stiffness (kN·mm <sup>-1</sup> )					Coefficient		
	$K_1$	$K_2$	$K_3$	$K_4$	$K_5$	$K_6$	$\lambda$	$l$
T-F	0.22336	0.08855	0.02280	-0.00333	$0.08062e^{-0.03996\Delta} + 0.0113e^{0.007884\Delta}$	$2.352\Delta^{-1.211} - 0.01682$	0.8	0.62
S-F	0.12945	0.02931	0.01047	-0.00128	$0.04553e^{0.002448\Delta} - 9.185e + 11e^{0.006446\Delta}$	$3896\Delta^{-2.865} - 0.007031$	0.9	0.57
Q-F	0.19852	0.05822	0.02398	0.01386	$0.1232e^{-0.01365\Delta} + 0.009221e^{0.0143\Delta}$	$7159\Delta^{-2.921} - 0.0072$	0.8	0.69

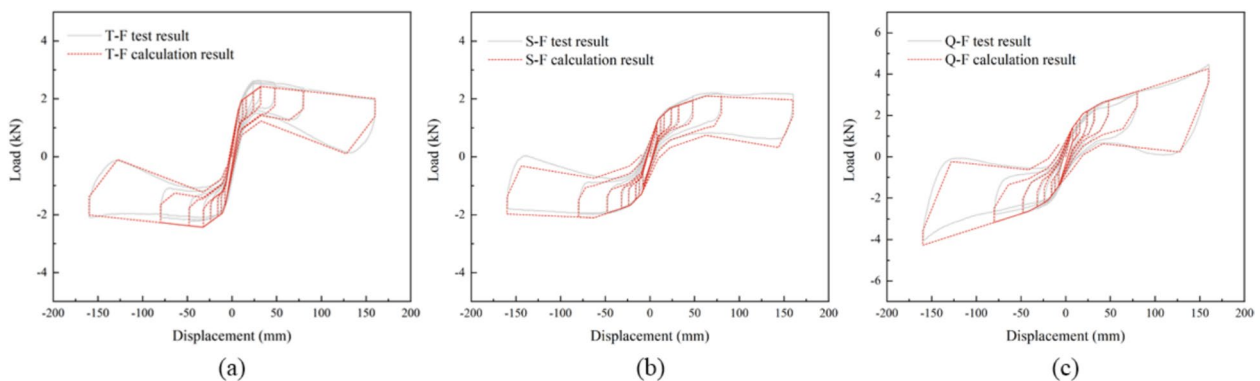


**Fig. 22** Comparison of calculated and test results

## Conclusions

This paper investigated the lateral resistance of three timber frames in ancient Chinese timber buildings. Quasi-static tests were conducted on three timber frames with different mortise–tenon joint connections to study the impact of these joints on the frames' lateral resistance. The main conclusions are as follows:

- (1) All three timber frames exhibited good deformation recovery capability. When the timber frames experienced significant horizontal lateral displacement, the mortise–tenon joints did not fail but produce plastic compressive deformation. Among the four types of joints, the *Gutou* mortise–tenon joint had the strongest ability to limit rotation and the best resistance to pull out. The *Zhi* mortise–tenon joint's ability to limit rotation was slightly lower than that of the *Niekou gumao* mortise–tenon joint and *Yanwei* mortise–tenon joint, and its resistance to pull out was also weaker than that of the *Niekou gumao* mortise–tenon joint at large horizontal loading displacements.
- (2) The hysteresis curves of the three timber frames all exhibited a swinging structure characteristic with full ends and pinched middles. However, due to the strong binding effect of the *Gutou* mortise–tenon joint, the maximum restoring force during the loading phase of the Q–F reached 1.76 times that of the T–F and 2.04 times that of the S–F.
- (3) The energy dissipation capacity of the three timber frames initially decreases and then increases with the increase of horizontal loading displacement. In addition, the extent of the increase in energy dissipation capacity for the three timber frames was related to the slip resistance of the mortise–tenon joints used, the stronger the slip resistance, the slower the increase in energy dissipation capacity. The different mortise–tenon joints caused different plastic deformations in the three timber frames during the loading process. Due to greater compressive and plastic deformations, the energy dissipation of the Q–F was significantly higher than that of the T–F and S–F.
- (4) A four-linear restoring force model suitable for timber frames with mortise–tenon joint connections between columns and *Fangs* was proposed. This model fit well with the test results and effectively reflected the restoring forces of timber frames using different mortise–tenon joints.

## Acknowledgements

We thank Suwan Dong, Yun Wang, Baolei Jin, Panpan Ma, and Fanxu Kong for their support in conducting the experiments.

## Author contributions

XL: designed and performed the experiments, analyzed the data, and writing of the manuscript. SW, ZC: designed and performed the experiments. ZQ, KK: writing—review and editing, supervision, funding acquisition. The manuscript was written through the contributions of all authors. All authors have given their approval to the final version of the manuscript.

## Funding

We gratefully acknowledge the financial support from the Japan Society for the Promotion of Science (JSPS) for this project.

## Availability of data and materials

The data sets used or analyzed during the current study are available from the corresponding author upon reasonable request.

## Declarations

### Competing interests

The authors declare that they have no competing interests regarding the publication of this paper.

Received: 6 September 2024 Accepted: 27 February 2025

Published online: 21 March 2025

## References

1. Gan X, Kong FX, Wang ZY, Li XR, Meng TY, Wang JY, Wang Q, Xie JQ, Que ZL (2024) Research on the lateral resistance of column frames in the Tang Dynasty: a case study of the straight tenon joints under varied vertical load levels. *Buildings* 15(1):25. <https://doi.org/10.3390/buildings15010025>
2. Chun Q, Yue Z, Pan JW (2011) Experimental study on seismic characteristics of typical mortise–tenon joints of Chinese southern traditional timber frame buildings. *Sci China Technol Sci* 54:2404–2411. <https://doi.org/10.1007/s11431-011-4448-3>
3. Li J (2011) *Yingzaofashi*. People's Publishing House, Beijing
4. Zhang SQ (ed) (2012) *Ningbo Baoguo temple hall: survey analysis and fundamental research*. Southeast University Press, Nanjing
5. Chen CC, Qiu HX, Lu Y (2016) Flexural behaviour of timber dovetail mortise–tenon joints. *Constr Build Mater* 112:366–377. <https://doi.org/10.1016/j.conbuildmat.2016.02.074>
6. Zhou Q, Yang N (2017) Typical structural health problems of tenon–mortise joints of ancient buildings in the Forbidden City. *J Water Resour Archit Eng* 15(05):12–19+38. <https://doi.org/10.3969/j.issn.1672-1144.2017.05.003>
7. Likos E, Haviarova E, Eckelman CA, Erdil YZ, Ozcifici A (2012) Effect of tenon geometry, grain orientation, and shoulder on bending moment capacity and moment rotation characteristics of mortise and tenon joints. *Wood Fiber Sci* 44(4):462–469
8. Li YZ, Cao SY, Xue JY (2016) Analysis on mechanical behavior of dovetail mortise–tenon joints with looseness in traditional timber buildings. *Struct Eng Mech* 60(5):903–921. <https://doi.org/10.1298/sem.2016.60.5.903>
9. Li SC, Chen LK, Jiang LZ, Li JQ (2020) Experimental investigation on the seismic behavior of the semi-rigid one-way straight mortise–tenon joint of a historical timber building. *Int J Archite Herit* 14(8):1135–1147. <https://doi.org/10.1080/15583058.2019.1587041>
10. Xue JY, Guo R, Qi LJ, Xu D (2019) Experimental study on the seismic performance of traditional timber mortise–tenon joints with different looseness under low-cyclic reversed loading. *Adv Struct Eng* 22(6):1312–1328. <https://doi.org/10.1177/1369433218814167>
11. Gao Z, Ma D, Wang Z, Guo X, Fang S, Fei Z (2021) Investigation of the restoring force model of through–tenon and half–tenon of timber with a certain level of universality. *BioResources* 16(3):5313–5328. <https://doi.org/10.15376/biores.16.3.5313-5328>
12. Li ZR, Isoda H, Kitamori A, Nakagawa T, Araki Y, Que ZL (2022) Analytical model for the capacities of traditional Japanese timber frames with deep beams. *Eng Struct* 253:113764. <https://doi.org/10.1016/j.engstruct.2021.113764>

13. Chang WS, Shanks J, Kitamori A, Komatsu K (2009) The structural behaviour of timber joints subjected to bi-axial bending. *Earthquake Eng Struct Dynam* 38(6):739–757. <https://doi.org/10.1002/EQE.854>
14. Li SC, Zhou ZC, Luo HZ, Milani G, Abuzzese D (2020) Behavior of traditional Chinese mortise-tenon joints: experimental and numerical insight for coupled vertical and reversed cyclic horizontal loads. *J Build Eng* 30:101257. <https://doi.org/10.1016/j.jobe.2020.101257>
15. Meng XJ, Yang QS, Wei JW, Li TY (2018) Experimental investigation on the lateral structural performance of a traditional Chinese pre-Ming dynasty timber structure based on half-scale pseudo-static tests. *Eng Struct* 167:582–591. <https://doi.org/10.1016/j.engstruct.2018.04.077>
16. Shi XW, Li TY, Chen YF, Chen JY, Yang QS (2018) Full-scale tests on the horizontal hysteretic behavior of a single-span timber frame. *Int J Archit Herit* 14(3):398–414. <https://doi.org/10.1080/15583058.2018.1547799>
17. Li XW, Zhao JH, Ma GW, Huang SH (2015) Experimental study on the traditional timber mortise-tenon joints. *Adv Struct Eng* 18(12):2089–2102. <https://doi.org/10.1260/1369-4332.18.12.2089>
18. Chen JY, Li TY, Yang QS, Shi XW, Zhao YX (2018) Degradation laws of hysteretic behaviour for historical timber buildings based on pseudo-static tests. *Eng Struct* 156:480–489. <https://doi.org/10.1016/j.engstruct.2017.11.054>
19. Zhang BZ, Xie QF, Liu YJ, Zhang LP, Li SY (2022) Effects of gaps on the seismic performance of traditional timber frames with straight mortise-tenon joint: experimental tests, energy dissipation mechanism and hysteretic model. *J Build Eng* 58:105019. <https://doi.org/10.1016/j.jobe.2022.105019>
20. Han M (2022) A brief analysis of methods for determining the age of ancient Chinese architecture. *Cult Ind* 36:87–89
21. Ma BJ (2003) Traditional techniques of timber construction in ancient Chinese architecture, 2nd edn. Science Press, Beijing
22. Maeno M, Suzuki Y, Matsumoto S (2007) Frame analysis based on modeling of structural characteristics in traditional wooden frames like temples. *Disaster Prevent Res Inst Ann* 50(B):117–131
23. Zhao C (ed) (2020) Timber frame shear wall structures: design and construction. China Architecture & Building Press, Beijing
24. Komatsu K, Kitamori A, Nakagawa T, Nakashima S, Isoda H (2023) Experimental study on the restoring force characteristics of traditional timber frame consisting of “Daitohijiki” (large bearing block with bracket arms), “Kasiranuki” (head tie-beams), and three circular columns and on the moment-resisting performance evaluated in each structural element. *J Struct Constr Eng, AIJ* 88(806):609–620. [https://doi.org/10.3130/aijs.88.609.\(InJapanese\)](https://doi.org/10.3130/aijs.88.609.(InJapanese))
25. Tanahashi H, Suzuki Y (2010) Elasto-plastic Pasternak model simulation of static and dynamic loading tests of traditional wooden frames. In: Proceedings of the 11th World Conference on Timber Engineering, Trentino, Italy, 20–24 June 2010.
26. Ministry of Housing and Urban-Rural Development, PRC (2015) Specification for seismic test of buildings (JGJ/T 101–2015). China Architecture & Building Press, Beijing
27. Wu YJ, Lin HS, Wang L, Xie QF, Zhang LP (2023) Influence of support interface on the lateral performance of rocking columns in traditional Chinese timber structures. *Structures* 48:2037–2047. <https://doi.org/10.1016/j.istruc.2023.01.094>
28. Tanahashi H, Suzuki Y (2020) Review on the mechanical models and formulations of embedment of traditional timber joints in Japan. *Jpn Archit Rev* 3(2):148–164. <https://doi.org/10.1002/2475-8876.12137>
29. Katagihara K (2001) Preservation and seismic retrofit of the traditional wooden buildings in Japan. *J Temporal Des Archit Environ* 1(1):12–20
30. Rinaldin G, Amadio C, Macorini L (2016) A macro-model with nonlinear springs for seismic analysis of URM buildings. *Earthquake Eng Struct Dynam* 45(14):2261–2281. <https://doi.org/10.1002/eqe.2759>

## Publisher's Note

Springer Nature remains neutral with regard to jurisdictional claims in published maps and institutional affiliations.